6-1-1992

Diurnal HO_2 cycles at clean air and urban sites in the troposphere

Thomas M. Hard
Portland State University

C. Y. Chan
Portland State University

A. A. Mehrabzadeh
Portland State University

Robert J. O'Brien
Portland State University

Citation Details

Hard, T. M., Chan, C. Y., Mehrabzadeh, A. A., & O'Brien, R. J. (1992). Diurnal HO_2 cycles at clean air and urban sites in the troposphere. Journal Of Geophysical Research, 97(D9), 9785-9794.

JOURNAL OF GEOPHYSICAL RESEARCH, VOL. 97, NO. D9, PAGES 9785–9794, JUNE 20, 1992

Diurnal HO_2 Cycles at Clean Air and Urban Sites in the Troposphere

T. M. HARD, C. Y. CHAN, A. A. MEHRABZADEH, AND R. J. O'BRIEN

Chemistry Department and Environmental Sciences and Resources Program, Portland State University, Portland, Oregon

We have determined HO_2 concentrations at two Oregon sites for continuous periods of 36 to 48 hours, using fluorescence assay with gas expansion. At the sea level coastal site (45°N 124°W), NNW winds prevailed during daytime, and a point measurement of very low total nonmethane hydrocarbon concentration indicated the presence of remote tropospheric air of oceanic origin. At the urban site, HO_2 was determined during moderately low ozone pollution levels. At both sites, maximum daily $[HO_2]$ was in the range of 1-2x10^8 cm^{-3} under clear-sky conditions, with an estimated overall uncertainty of 40%. HO_2 was detected by continuous low-pressure sampling with flowing chemical conversion to HO, which was detected by laser-excited fluorescence. The instrumental response to HO_2 was calibrated by the self-decay of HO_2 at atmospheric pressure. Interference in the measured daytime HO_2 concentrations by RO_2 was estimated at less than 20%.

INTRODUCTION

Hydroperoxyl radical, HO_2, is created by the tropospheric photooxidation of hydrocarbons, carbon monoxide, and hydrogen, whose sources are both biospheric and human-made. This oxidation is initiated by chemical reactions of the latter species with the closely related free radical, HO. Partially oxidized hydrocarbons, such as formaldehyde, are photodissociated by sunlight to yield HO_2. These reactions can lead to tropospheric ozone production, for which HO_2 is an essential intermediate.

Anderson et al. [1981] and *Stimpfle et al.* [1990] determined HO_2 in the upper stratosphere by converting it to HO via NO addition, detecting the product HO by the fluorescence excited with an HO resonance lamp. *Traub et al.* [1990] detected stratospheric HO_2 between 23 and 49 km by balloon-borne far-infrared emission spectroscopy, and *Mihelcic et al.* [1990] determined HO_2 by electron-spin resonance (ESR) in cryogenic matrix samples collected in the troposphere. *Hard et al.* [1984] measured HO_2 near ground level in urban air by low-pressure conversion to HO, using laser-excited fluorescence (LEF) with chemical modulation.

In measurements of related species, *Mihelcic et al.* [1978, 1985, 1990] measured RO_2 (R = organic radical) by ESR in both stratospheric and tropospheric matrix samples. *Cantrell and Stedman* [1982] measured $HO_2 + \Sigma_i a_i[RO_2]_i$ by chemical amplification of NO conversion; here a_i represents the ability (relative to HO_2) of the ith RO_2 species (and its subsequent products) to oxidize NO to NO_2 under the chosen NO and CO reagent conditions. *Parrish et al.* [1986] measured the imbalance in the atmospheric $NO\text{-}NO_2\text{-}O_3$ photochemical steady state under a wide variety of conditions. Parrish et al. assigned excesses in the NO_2-to-NO ratio to species represented by HO_2 and RO_2, which produce ozone, and to unidentified free radicals which are neutral with respect to net O_3 production.

Paper number 92JD00232.
0148-0227/92/92JD-00232$05.00

In the present work HO_2 is determined by fluorescence assay with gas expansion (FAGE) [*Hard et al.*, 1984, 1986, 1992; *Chan et al.*, 1990], a method which employs low-pressure laser-excited fluorescence to observe the hydroxyl radical HO, using chemical modulation to distinguish the desired signal from the background. In the HO_2 determination mode, NO is added to the low-pressure flowing sample, converting HO_2 to HO:

$$\text{(R1)} \qquad HO_2 + NO \rightarrow HO + NO_2$$

The efficiency of the HO_2-to-HO conversion is discussed below.

Ambient HO_2 was measured at two Oregon sites, one coastal and the other inland urban. The coastal site sampled sea level North Pacific air which was free from local pollution sources under suitable wind conditions. The urban site (downtown Portland) was subject largely to automotive pollutant sources.

KINETIC PRINCIPLES OF FAGE HO_2 DETERMINATION

The efficiency of HO_2 detection as HO following (R1) is limited by another reaction also driven by the NO reagent:

$$\text{(R2)} \qquad HO + NO + M \rightarrow HONO + M$$

Thus the yield of HO from the above mechanism is pressure dependent via M, and low-pressure conditions are most effective for HO_2 determination.

In the present method a constant NO flow is added to both air sampling channels of FAGE. The signal from the HO product is turned on and off (modulated) in each sample channel by addition of isobutane (i-C_4H_{10}, here called i-BuH) to the flow, alternating between the two channels, via

$$\text{(R3)} \qquad HO + i\text{-}C_4H_{10} \rightarrow H_2O + C_4H_9$$

Earlier [*Hard et al.*, 1984] we used NO alone as the modulating reagent, similarly to the approach of *Anderson et al.* [1981] and *Stimpfle et al.* [1990]. The reason for the change to chemical modulation by isobutane is to avoid possible interferences, discussed in a later section. The isobutane also modulates ambient HO via (R3), with somewhat higher overall efficiency, but the resulting small HO signal is comparable with the measurement uncertainty of the much more abundant HO_2.

At the LEF detection zone, the conversion efficiency of HO_2 to HO is

$$E_c = [HO]/[HO_2]_0 \quad (1)$$
$$= \{\exp(-k_1[NO]t_r) - \exp(-k_2[NO][M]t_r - k_3[i\text{-BuH}]t_r)\} \times k_1[NO]/(k_2[NO][M] + k_3[i\text{-BuH}] - k_1[NO])$$

where $[HO_2]_0$ is the initial HO_2 concentration after expansion to low pressure and t_r is the transit time from the nozzle to the detection zone. Equation (1) is obtained by successive integration of the differential equations for $[HO_2]$ and [HO] with respect to time from the nozzle exit (t=0) to t_r [*Hard et al.*, 1984]. Under real flow conditions, t_r is not constant with radial position in the sample flow at the detection zone, and highest flow rate occurs along the tube axis. Given sufficient information on the flow field, an area-weighted value of E_c could be calculated for the common intersection of the sample flow, laser beam, and detector mask image. Instead, we have obtained an effective value of t_r = 16 ms (±25%) from the measured modulation of external HO by isobutane in the absence of NO [*Hard et al.*, 1992]; the error limits are due largely to uncertainty in the HO+isobutane reaction rate coefficient. For the latter value we have used $k_3 = 2.5\times10^{-12}$ cm^3 molec^{-1} s^{-1} [*Greiner*, 1970; *Darnall et al.*, 1978](molec = molecules). The observed value of t_r is somewhat closer to the expected transit time for the core of laminar flow, 12.5 ms, than to the hypothetical plug-flow residence time, 25 ms. Here we should stress that t_r and E_c need not be known accurately, since the overall response of the FAGE instrument to HO_2 is obtained independently by external calibration; however, t_r and E_c are useful for instrument description and the estimation of upper limits to the possible interferences.

Equation (1) assumes pseudo-first-order reaction of HO_2 in (R1), and of HO in (R2) and (R3). The reagent mole fractions used in these experiments (see below) exceed those of HO_2 and HO by at least a factor of 10^6, so this condition is clearly fulfilled.

The behavior of equation (1) is plotted in Figure 1 as a function of reaction time t_r at the NO concentration used in our experiments, without isobutane (E_{c0}, top curve) and modulated with isobutane (E_{ci}, bottom curve). The net HO_2 signal is proportional to the difference between the two curves at the transit time t_r. The vertical lines indicate the laminar, observed, and plug-flow transit times just discussed. Without isobutane, reaction (R2) limits the maximum achievable conversion efficiency of HO_2 to HO:

$$(E_{c0})_{max} = \left(\frac{k_2[M]}{k_1}\right)^{\frac{k_2[M]}{k_1 - k_2[M]}} \quad (2)$$

This maximum value of E_{c0} occurs at a value of [NO] given by

$$[NO((E_{c0})_{max})] = (1/t_r)\ \ln(k_1/k_2[M]) \ / \ (k_1 - k_2[M]) \quad (3)$$

Equations (2) and (3) are obtained by differentiating equation (1) with respect to t_r and setting the derivative of E_{c0} equal to zero [*Hard et al.*, 1984].

With currently recommended values of k_1 and k_2 [*Atkinson et al*, 1989], the value of $(E_{c0})_{max}$ is 94% at 4 torr. In the present experiments, we used an NO concentration $[NO]_{std} < [NO((E_{c0})_{max})]$ to minimize interferences discussed in a later section.

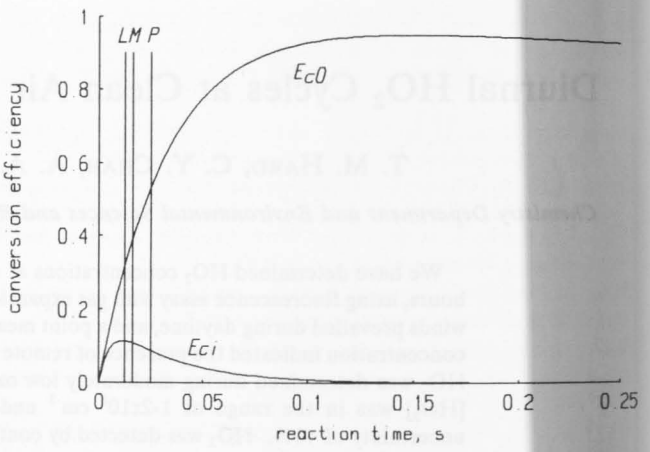

Fig. 1. Conversion efficiency of HO_2 to HO versus transit time in FAGE probe. Top curve: with standard [NO] used in HO_2 determination, this curve represents the theoretical gross HO_2 signal. Bottom curve: same, with standard isobutane concentration, this curve represents the theoretical background signal. The net signal due to HO_2 is the difference (at any transit time) between these two curves. Vertical lines: L, residence time of core of laminar flow; P, plug-flow residence time; M, observed residence time [*Hard et al.*, 1992].

For the HO produced by (R1), the modulation efficiency at the transit time t_r, due to isobutane injection, is

$$E_{mod} = 1 - E_{ci} \ / \ E_{c0} \quad (4)$$

Neglecting wall losses of HO_2 and HO, the overall chemical efficiency E_{chem} with which a net HO_2 "signal" is produced is

$$E_{chem} = E_{c0}E_{mod} = E_{c0} - E_{ci} \quad (5)$$

E_{chem} and E_{mod} are plotted against [NO] in Figure 2. We emphasize again that equations (1) through (5) are used only to describe instrumental behavior and to aid in the selection of reagent concentrations and are not needed for calibration of the instrument's response to ambient HO_2. A

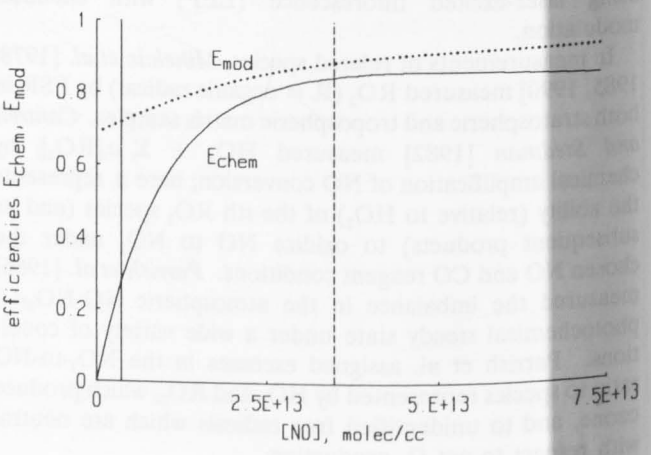

Fig. 2. HO_2 to HO conversion efficiencies versus NO. Dotted curve is E_{mod}, the efficiency of modulating the HO_2 to HO signal with isobutane; solid curve is E_{chem}, the chemical efficiency with which a net HO_2 signal is produced as HO (see text or Table 1 for definitions of efficiencies). Vertical solid line is $[NO]_{std}$, the NO concentration used in these measurements. Vertical dashed line: [NO] giving maximum conversion efficiency $(E_{c0})_{max}$. (Read 2.5E+13 as 2.5×10^{13}.)

summary of the efficiency terms just defined is given in Table 1.

EXPERIMENT

The HO_2 instrument is a modification of the FAGE instrument described earlier [*Hard et al.*, 1984, 1986] designed to measure both HO and HO_2. *Hard et al.* [1992] provide a detailed description of the FAGE2 instrument used in these experiments. For the "clean air" experiments, the instrument was installed in a converted motor home used as a field research vehicle. These experiments were performed in August 1987 at our Pacific coastal site (45°N 124°W). The HO_2 sampling point was located 7 m horizontally and 5 m vertically from mean high tide. The site, in Lincoln City, Oregon, was a compromise between the desire for a remote site and the need for three-phase electrical power. Under suitable weather conditions, which were present during part of our measurement period, offshore winds brought remote North Pacific air to the coastal site, as evidenced by hydrocarbon analysis discussed below.

The urban HO_2 data were obtained in August 1986 at a rooftop site at Portland State University in downtown Portland, Oregon. This site was used earlier for the ambient HO measurements of June and November 1985 with FAGE2 [*Hard et al.*, 1986], and for the ambient HO and HO_2 measurements of August and October 1983 with FAGE1 [*Hard et al.*, 1984].

The 30-Hz Nd:YAG-pumped Rh6G dye laser (Quantel YG580 + TDL50) was frequency-doubled and tuned to the $Q_1 1,1' + R_2 3$ line group of the $A\ ^2\Pi\ (v'=1) \leftarrow X\ ^2\Sigma\ (v''=0)$ band of HO at 282 nm. The instrumental conditions were the same as those described for HO determination [Hard *et al.*, 1992], except for the methods of chemical modulation and calibration.

In HO measurements with FAGE, the isobutane modulating reagent is admitted in a carrier gas (air) to the 8 L/min sample flow about 5 mm downstream from the entrance of each nozzle through three small inlets at 120° intervals, flush with the interior wall and connected via a low-volume manifold. In HO_2 determination, the 200 mL/min N_2 carrier gas transported the reagent NO continuously to both sample probes. The NO reagent flow (Scientific Gas Products, 5% in N_2) was filtered by NaOH pellets, Ascarite, and $FeSO_4$, to remove N oxides and oxyacids. The constant NO flow was regulated by a Tylan mass flow controller; the resulting NO concentration in the flow tubes was $[NO]_{std} = 3.7\times10^{12}$ cm^{-3}. A controlled flow of isobutane (Matheson instrument grade, 99.5%), was delivered alternately to the two probes, in order to modulate the HO (produced from HO_2 by reaction (R1)) by chemical removal [*Hard et al.*, 1984, 1986, 1992]. As in [HO] determination, the pressure in the sample tubes and detection zone was 4 torr.

The ambient UV irradiance (290-400 nm) was monitored by a Si photoconductor filtered by a Corning 9863 filter, facing the zenith. Ozone was monitored by its UV absorption (Dasibi 1003-AH). H_2O was measured with a dewpoint hygrometer (General Eastern 1100DP). The NO monitor (Thermo-Electron model 12) had not yet been modified for clean-tropospheric NO determination purposes at the time of this experiment; thus its output revealed only those periods when the data were influenced by local combustion sources. Wind direction and speed were provided by a vane and an anemometer connected to a small weather station (Heathkit ID-4001) and were converted to S→N and W→E vector components for averaging by the computer. Hydrocarbon samples were taken on the van's roof, using evacuated stainless steel canisters kindly offered by James Greenberg of the National Center for Atmospheric Research

TABLE 1. Glossary of HO_2 Measurement Quantities

Term	Definition	Equation
E_c	conversion efficiency of HO2 to HO as a function of FAGE pressure (expressed as number density [M]), added [NO], probe transit time t_r, and added modulating reagent concentration [*i*-BuH]	(1)
E_{c0}	conversion efficiency without isobutane*: efficiency for producing the gross HO_2 signal	(1)
E_{ci}	reduced conversion efficiency with isobutane*, used for background measurement	(1)
[M]	flow tube number density, equivalent to 4 torr under standard flow tube operating conditions	(1)
$(E_{c0})_{max}$	maximum achievable HO_2 conversion efficiency (not optimal, since RO_2 interference is proportionately less at lower conversion efficiencies; see Figure 6)	(2)
$[NO(E_{c0})_{max}]$	nitric oxide concentration required to give maximum HO2 conversion efficiency	(3)
E_{mod}	efficiency of modulation (by isobutane) of HO produced from HO_2	(4)
E_{chem}	overall chemical efficiency with which a net HO_2 signal is produced as HO	(5)
r	measured response factor for HO_2, photons per unit time per unit ambient HO_2 concentration	(6)
s_1	slope of inverse signal versus time curve in HO_2 self-calibration (e.g., Figure 5*a*)	
$[NO]_{std}$	standard flow-tube nitric oxide concentration used in these experiments for reduction of HO_2 to HO: 3.7×10^{12} cm^{-3}.	

*The net HO_2 signal efficiency as HO is the difference $E_{c0} - E_{ci}$.

(NCAR), who also provided hydrocarbon and CO analyses of these samples.

For the HO_2 + HO_2 self-calibration procedure, the initial HO_2 concentration was provided by UV irradiation of CH_2O vapor in dry air in a continuously stirred tank reactor (CSTR), made of fluoro-ethylene polymer (FEP) teflon film. Air in the reactor was sampled continuously by the two FAGE nozzles. The air flow into the CSTR was provided by a pure-air generator (AADCO 20 L/min); a small fraction of the flow (120 mL/min) was bubbled through CH_2O in water in contact with the solid polymeric form (MCB, containing 12% CH_3OH as stabilizer) maintained at 0°C by an ice bath. The pure-air generator yielded air with an upper-limit dewpoint of less than −18°C. The vapor pressure of the liquid H_2O in the CH_2O source at 0°C was 4.6 torr, but the flow through this bubbler was a negligible fraction of the total. After mixing of these unequal air streams, the partial pressure of H_2O in the CSTR was less than 1 torr, due largely to any residual water vapor passing through the pure-air generator. During irradiation, the temperature of the reactor was 1° to 2°C warmer than the surrounding air. After steady state HO_2 signals were observed, the UV lamps and the stirring fan were turned off, and the resulting HO_2 signal decay was recorded over a period of 3 min. To secure a useful second-order region of the decay curve the following precautions were found necessary. Teflon bags previously used for hydrocarbon-loss calibration of HO response [*Hard et al.*, 1986; *Chan et al.*, 1990] were found unsatisfactory for HO_2 calibration. (The likely cause for the this problem was wall-stored mesitylene-NO_x photooxidation products (e.g., sources of RO_2 radicals), desorbing and reacting with HO_2, competing with the desired second-order self-reaction of HO_2. When the calibration was performed outdoors, exclusion of daylight was necessary; otherwise new HO_2 production interfered with the desired decay. An alternative HO_2 source, photolysis of Cl_2 in an H_2 + air mixture, gave much higher [HO_2], but the early portion of the decay curve was non-second order, suggesting release of HO_2 from a reservoir species such as H_2O_4 [*Sander et al.*, 1982; *Fitzgerald et al.*, 1985] accumulated during the steady state preparation of HO_2. In contrast, at the much lower initial HO_2 concentrations prepared with the CH_2O photolysis system, the early and middle portions of the decay agreed, indicating negligible contribution from thermal dissociation of reservoirs. A further disadvantage of the Cl_2-H_2 system, absent in CH_2O photolysis, was corrosion of the metallic outer parts of the nozzle by the HCl product.

RESULTS AND DISCUSSION

Ambient Data

Ambient HO_2 data, obtained at our coastal Oregon site during August 24-26, 1987, are shown in Figure 3. A strong diurnal variation of HO_2 under sea level conditions is evident. The 6-min averaging time is one-tenth of that used in our report of the HO diurnal cycle at this site [*Hard et al.*, 1992], made possible by the nearly 100-fold greater radical concentration observed here.

Winds exhibited a typical diurnal pattern for this site, moderate NW to NNW during the day, and falling to low speeds during the night (bottom panel of Figure 3). Offshore fog was present during this period, enveloping the

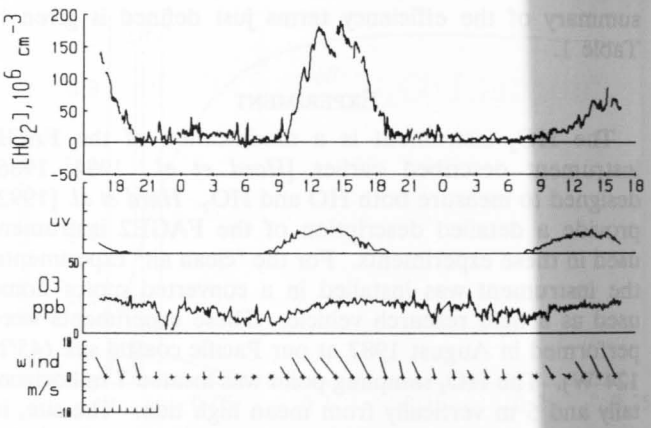

Fig. 3. Coastal HO_2 data, August 24-26, 1987, Lincoln City, Oregon, plotted with 0.1 hour averaging time. Abscissa in hours, Pacific daylight time. The vertical error bar represents ±2 times the average of the tenth-hourly standard errors of the mean [HO_2] data. Continuous ultraviolet light intensity (UV) in arbitrary units, see text.

site at night, and persisting until 0830 LT (local time, Pacific Daylight Time) on the 25th and throughout the 26th. On the 26th, visual observation, confirmed by the UV data in Figure 3, indicated that the daytime fog was bright, and therefore the fog layer was shallow.

Ozone showed a weak diurnal variation, indicating low impact of local emissions. Nocturnal wind reversal often brings much lower nighttime ozone to this site. During daytime periods, ozone remained between 20 and 25 ppb.

As mentioned above, the NO measurements were only sensitive enough to detect intrusion of land-based sources. Peaks in NO coincided with E winds and reductions in O_3, which occurred sporadically between 2200 LT and 1000 LT on both nights. H_2O (not shown in Figure 3) was in the 8 to 11 torr range.

One hydrocarbon grab sample was taken during the period covered by Figure 3, at 1525 LT on August 25, and its analysis (provided by James Greenberg, NCAR) is given in Table 2. This sample shows total nonmethane hydrocarbon (TNMHC) concentrations (6.3 ppbvC) that are very low compared to continental and even some remote maritime levels (see, for instance *Greenberg and Zimmerman* [1984]). Listed for comparison are data from the samples nearest in time (afternoons of August 22 and 27). In the latter samples, TNMHC were 2-4 times higher and C_3-C_5 hydrocarbons may have been increased by emissions from a restaurant kitchen whose vents were 30 m N of our sampling point.

In Figure 3, there is a morning lag of at least 2 hours between the rise of ambient UV levels and that of daytime HO_2. The HO_2 rise corresponds to an increase in the speed of the west component of the wind. Such behavior might be explained by the occurrence of nocturnal temperature inversions. HO_2 is believed to increase with altitude in the lower troposphere [*Logan et al.*, 1981]. Horizontal wind speed, as well as vertical mixing rates, are weaker during the night; morning breakup of an inversion occurs after sufficient heating by the Sun. This leads 1) to the removal of fog droplets (removing a known HO_2 sink [*Chameides and Davis*, 1982; *Schwartz*, 1984; *Jacob*, 1986; *Mozurkewich et al.*, 1987; *Lelieveld and Crutzen*, 1990]) and 2) to a possible

TABLE 2. Hydrocarbon Analysis Summary

	August 22, 1987	August 25, 1987	August 27, 1987
methane	1772	1705	1696
CO	156	113	202
ethane	0.73	0.58	0.61
ethene	0.17	0.36	0.43
ethyne	0.98	0.04	nd
propane	0.50	0.07	0.40
propene	0.03	0.11	0.30
propyne	nd	nd	nd
isobutane	0.27	nd	0.19
n-butane	0.98	nd	0.50
butenes	nd	nd	nd
isopentane	0.93	0.03	0.27
n-pentane	0.39	nd	0.15
pentenes (total)	0.09	nd	0.29
isoprene	0.06	nd	0.06
other alkanes	0.50	0.03	0.15
other alkenes	0.17	0.10	0.35
aromatics (total)	0.45	0.34	0.46
benzene	0.15	0.03	0.09
toluene	0.15	0.21	0.14
terpenes	0.03	0.03	nd
TNMHC, ppbvC	25.8	6.3	14.8

Hydrocarbon analyses by James Greenberg, National Center for Atmospheric Research. Units are parts per billion by volume of compound in air, except for TNMHC, whose units are parts per billion by volume of carbon (atoms) in air (molecules). The abbreviation nd means not detected.

increase in vertical mixing, introducing HO_2 from the region above the inversion.

Figure 4 shows ambient HO_2 data observed in urban air during the period August 26-27, 1986, at our rooftop site in downtown Portland Oregon. The first afternoon of this period (from 1500 LT) shows the latter half of a diurnal cycle in HO_2 whose peak concentration is similar to that of the clean air measurements of Figure 3. The second day in Figure 4 was partially cloudy, as indicated by the spikes in the relative UV light intensity. Measured HO_2 concentrations are lower on the second day, consistent with higher NO levels during this period. Significant nighttime HO_2 signals occur during a period of 4 hours when $[O_3] > [NO]$ on the first night. In contrast, HO_2 signals are quite low during the second night, which had elevated NO concentrations at all times.

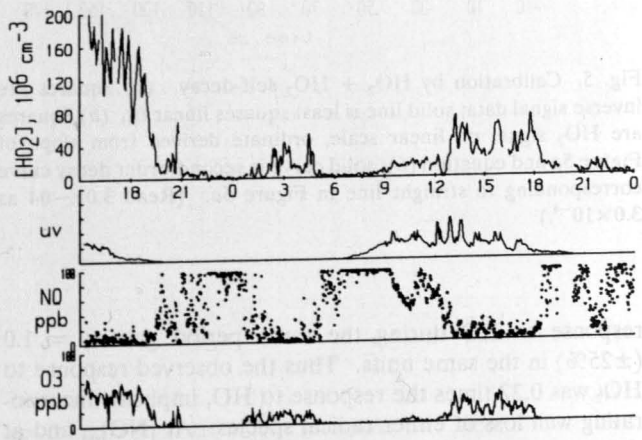

Fig. 4. Rooftop HO_2 data, August 26-27, 1986, downtown Portland, Oregon, plotted with 0.1 hour averaging time. Abscissa and UV units same as in Figure 3.

Calibration

The decay of HO_2 in the dark due to the parallel reactions

$$\text{(R4}a\text{)} \qquad HO_2 + HO_2 \rightarrow H_2O_2 + O_2$$

$$\text{(R4}b\text{)} \qquad HO_2 + HO_2 + M \rightarrow H_2O_2 + O_2 + M$$

is used to calibrate the HO_2 response of FAGE. The net rate coefficient $k_{4a}+k_{4b}$ at 1 atm and 298 K is given as 2.9×10^{-12} molec^{-1} cm^3 s^{-1} in the review by *Atkinson et al.* [1989], and this rate coefficient is accelerated by 7.4% per 1 torr of H_2O vapor, which is the upper limit to its partial pressure in the calibration chamber. Since (R4*a*) and (R4*b*) are second order with respect to HO_2, a plot of the inverse of the decaying fluorescence signals (after background subtraction, and in arbitrary units) versus time should give a linear least squares fit, yielding a slope s_1, as in Figure 5*a*.

The response r (in photons per unit time per unit HO_2 concentration) is given by

$$r = 2(k_{4a}+k_{4b})/s_1. \qquad (6)$$

The same decay is plotted on a linear scale in Figure 5*b*, where equation (6) has been used to convert the signal to HO_2 concentration. Deviation of the final portion of the decaying signals from the least squares line in Figure 5*a* is ascribed to first-order reactions of HO_2 with CH_2O and/or with trace contaminants. Several decay experiments were performed in succession, and their results were averaged to obtain a value of $r = 0.22$ (±30%) photons s^{-1} (1×10^6 radicals cm^{-3})$^{-1}$. Moreover, calibration of the FAGE

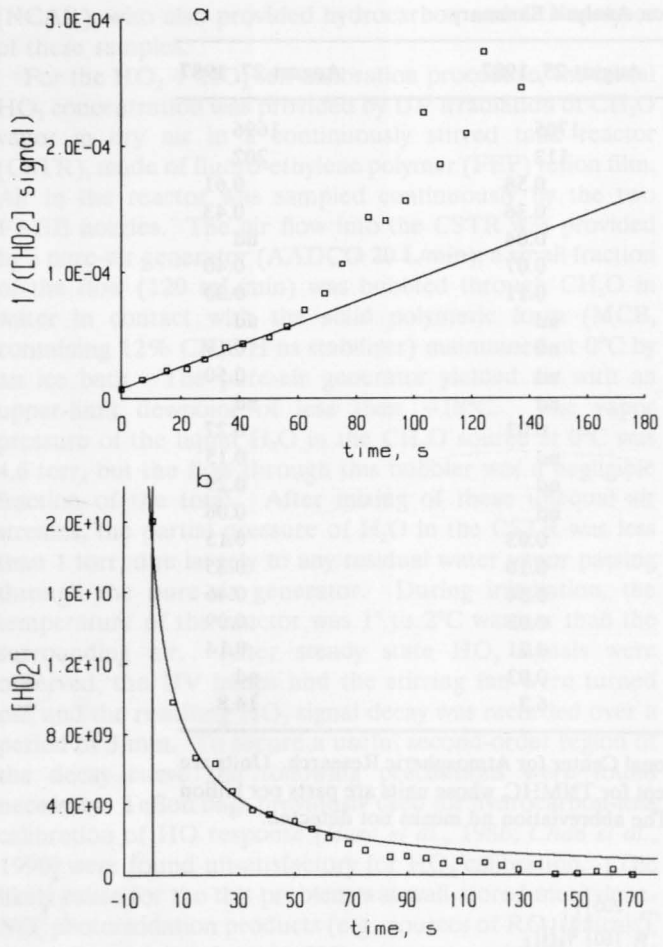

Fig. 5. Calibration by $HO_2 + HO_2$ self-decay. (*a*) Squares are inverse signal data; solid line is least squares linear fit. (*b*) Squares are HO_2 signal on linear scale, ordinate derived from slope of Figure 5*a* and equation (6); solid curve is second-order decay curve corresponding to straight line in Figure 5*a*. (Read 3.0E−04 as 3.0×10^{-4}.)

response to HO during the same period gave $r = 1.0$ (±25%) in the same units. Thus the observed response to HO_2 was 0.22 times the response to HO, implicitly incorporating wall loss of either radical species. At $[NO]_{std}$ and at the measured residence time, the product of the calculated chemical conversion and modulation efficiencies of HO_2 is 0.28 (±25%) (Figure 2), while that of HO is 0.95 (±3%) [*Hard et al.*, 1992]. Thus the ratio of the predicted chemical signal efficiencies of the two species is 0.28/0.95 = 0.295, which is about 33% greater than the ratio of the observed responses. It would not be surprising if HO_2 had a lower chemical signal efficiency, due to a higher removal rate of HO (following HO_2 conversion to HO) at the flow tube walls in the presence of the relatively large (and constant) flow of NO employed for reduction of HO_2 to HO (i.e., by HO+NO → HONO). In contrast, any heterogeneous reaction of HO_2 would be expected as reduction to HO by NO at the flow tube walls.

Interferences

1. Other peroxy radicals (RO_2), where R is an organic radical, are a potential source of interference in the determination of HO_2, via

(R5*a*) $RO_2 + NO \rightarrow RO + NO_2$

(R5*b*) $RO_2 + NO \rightarrow RONO_2$

(R6) $RO + O_2 \rightarrow R'CHO + HO_2$

followed by HO production via (R1) and (R2) and chemical modulation via (R3). If RO_2 = alkylperoxy, then (R6) is somewhat faster than (R5*a*) at the 4 torr detection pressure, but not fast enough to be treated as instantaneous, as assumed in our previous treatment [*Hard et al.*, 1984]. Moreover, at the NO concentration $[NO]_{std}$ used here for HO_2 conversion, the reactions

(R7*a*) $RO + NO + M \rightarrow RONO + M$

(R7*b*) $RO + NO \rightarrow R'O + HNO$

compete with (R6), reducing subsequent HO_2 production, resulting in lower calculated RO_2 interference. Implicit integration of the differential equations for RO_2, RO, and their HO_2 and HO products, with R=CH_3, C_2H_5, *n*-C_3H_9, and *i*-C_3H_9, allows calculation of the respective RO_2 net chemical signal efficiencies in chemical modulation by isobutane, relative to E_{chem} of ambient HO_2. The latter ratios are plotted in Figure 6 as functions of reagent [NO]. These calculations conservatively used the plug-flow transit time of t_r = 25 ms to calculate upper limits to the RO_2 interference; the actual transit time (Figure 1) is about 40% shorter [*Hard et al.*, 1992]. The $C_2H_5O_2$ and (*n*,*i*)-$C_3H_9O_2$ radicals give approximately the same efficiency curve, which is somewhat higher than that of CH_3O_2. Acylperoxy radicals (RCO_3) produce much less interference than RO_2 at $[NO]_{std}$ since they must undergo two additional kinetic steps to yield HO:

(R8) $RC(=O)OO + NO \rightarrow R + CO_2 + NO_2$

(R9) $R + O_2 \rightarrow RO_2$

followed by the sequence of reactions (R5), (R6), and (R1). The resulting interference versus [NO] for the case of acetylperoxyl radical (R = CH_3) is shown in the bottom curve of Figure 6. At $[NO]_{std}$, we obtain relative signal efficiencies $(E_{chem})_{RO2}/(E_{chem})_{HO2}$ for CH_3O_2, the C_2 and C_3

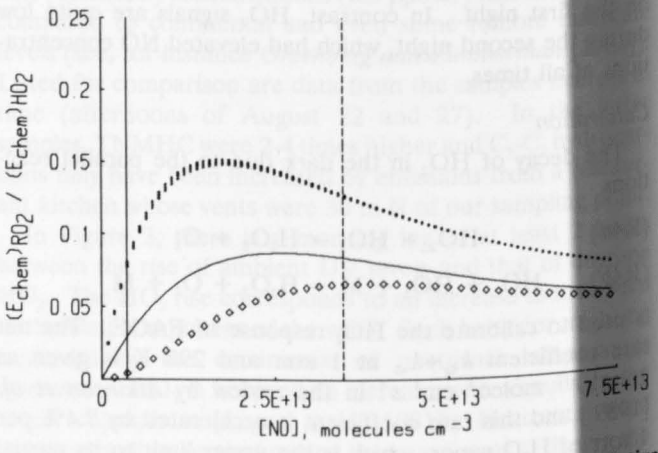

Fig. 6. Overall chemical signal efficiencies of RO_2 species relative to HO_2, as a function of [NO]. Solid curve is R=CH_3, dotted curves are R=C_2H_5, *n*-C_3H_7, *i*-C_3H_7, diamonds show $CH_3C(=O)OO$ as an example of acylperoxy radical behavior. Vertical solid line is $[NO]_{std}$. Vertical dashed line is [NO] giving maximum HO_2 conversion efficiency $(E_{c0})_{max}$. (Read 2.5E+13 as 2.5×10^{13}.)

alkylperoxy radicals, and CH_3CO_3 of 0.03, 0.08, and 0.004, respectively.

To predict interference from RO_2, representative $[RO_2]/[HO_2]$ ratios in ambient air are necessary. Our previous discussion [*Hard et al.*, 1984] attempted to set an upper limit of less than 1 to this ratio by comparing $\Sigma_i k_{5ai}[RO_2]_i$ with $k_1[HO_2]$ at steady state, since the sources of HO_2 include not only the reaction chain (R5*a*) + (R6) but also aldehyde photolysis and the reactions of HO with CO, H_2O_2, and H_2. That upper limit is supported further by competition for the RO_2 and RO intermediates by reactions (R5*b*), (R7*a*), and (R7*b*). However, the postulated limit fails when ambient air is not in photochemical steady state, at night in particular, or when reaction with NO is not the predominant fate of HO_2. The limit appears to be valid in the daytime for remote air (assuming insignificant nonmethane hydrocarbons) at 45°N at all tropospheric altitudes at the equinox [*Logan et al.*, 1981]. At ground level the latter authors predict midday-maximum and nighttime CH_3O_2/HO_2 ratios of 0.25 and ~10, respectively. For tropical ground-level equinoctial conditions, radical-radical recombination paths which remove RO_2 and HO_2 are predominant and lead to higher CH_3O_2/HO_2 ratios [*Logan et al.*, 1981].

Recently, *Madronich and Calvert* [1990] have examined the possible influence of peroxy radical self-reactions (RO_2+RO_2) on the chemistry of the marine (40°N, equinox) and Amazon (equator, July 1) planetary boundary layer (PBL). Their modeling effort studied the effect of permutation reactions on the concentrations of HO_2 and a variety of RO_2 species. Such reactions tend to raise HO_2 and lower RO_2. Radical concentrations were tabulated for noon of a 5-day simulation with and without continuous emission sources, and with and without the permutation reactions included in the model. For the most realistic case, which includes both permutations and emission sources, the model yielded HO_2, alkylperoxy, and acylperoxy radical concentrations of 3.2×10^8, 7.6×10^8, and 1.0×10^8 molecules cm^{-3}, respectively, for the marine PBL. For the Amazon PBL simulation the respective concentrations were 1.1×10^9, 4.6×10^9, and 7.9×10^9. Assuming that $(E_{chem})_{C2H5O2}$ and $(E_{chem})_{CH3CO3}$ are representative of the alkylperoxyl and acylperoxyl radicals, respectively, the resulting interferences by these radicals at noon are 20% and 0.1% of $[HO_2]$ in the 40°N marine PBL and 33% and 1% of $[HO_2]$ for the Amazon PBL. These calculations are summarized in Table 3.

Donahue and Prinn [1990] modeled NMHC chemistry for the tropical (15°S) remote marine boundary layer (MBL). For their "base case," their Figures 6 and 7 provide the approximate daytime maximum and nocturnal radical concentrations listed in the bottom half of Table 3. A major uncertainty in these radical results arose from the fluxes of heavy alkenes, for which there were insufficient experimental concentration data. To estimate interferences, we lump the primary, secondary, and tertiary alkylperoxyl radical concentrations and assume their effective value of E_{chem} is that of $C_2H_5O_2$. Then the estimated daytime maximum interferences by CH_3O_2, nonmethane RO_2, and RCO_3 are 5%, 14%, and 0.2%, respectively, and 12%, 54%, and 0.08% at night. Thus the total RO_2 interferences we estimate for Donahue and Prinn's tropical marine conditions are 20% of $[HO_2]$ at the daytime peak and 66% at night. If similar behavior were to hold for the midlatitude MBL at 45°N, then the small residual signals observed at night in Figure 3 would be due primarily to RO_2.

2. Reversible thermal dissociation of HNO_4 (HO_2NO_2), which yields HO_2 when the sample pressure is reduced, is a potential source of HO_2 interference. High steady state values of the ambient $[HNO_4]/[HO_2]$ ratio correspond with low temperatures and high $[NO_2]$. For example, under the extreme conditions of 273 K and 1 ppm NO_2 at ground level, we calculate $[HNO_4]/[HO_2] = 1.2\times10^4$ in the air

TABLE 3. RO_2 Interferences Calculated From Model Predictions of Ambient $[HO_2]$ and $[RO_2]$

Species	Relative Efficiency[a]	40°N MBL, Noon[b]	Interference[c]	Amazon, Noon[d]	Interference
HO_2	1.0	3.2E8[e]		1.1E9	
alkylperoxy	0.08	7.6E8	0.19	4.6E9	0.33
acylperoxy	0.0044	1.0E8	0.001	7.9E9	0.01
total			0.19		0.34
Species	**Relative Efficiency**	**15°S MBL, Noon[f]**	**Interference**	**15°S MBL, Night[f]**	**Interference**
HO_2	1.0	4.E8		5.E7	
CH_3O_2	0.03	7.E8	0.05	2.E8	0.12
RCH_2O_2	0.08	3.E8		3.E8	
R_2CHO_2	0.08	3.5E8	0.14[g]	3.5E7	0.54[g]
R_3CO_2	0.08	3.E7		2.5E6	
RCO_3	0.0044	2.2E8	0.002	9.E6	0.0008
total			0.19		0.66

[a] Overall chemical efficiency of conversion and modulation in FAGE2, normalized to that of HO_2. For alkylperoxy radicals the efficiencies are assumed equal to that of ethylperoxyl.
[b] *Madronich and Calvert* [1990], 40°N marine boundary layer, equinox.
[c] Interference relative to concurrent HO_2 signal.
[d] *Madronich and Calvert* [1990], Amazon boundary layer, July 1.
[e] Read 3.2E8 = 3.2×10^8 radicals cm^{-3}.
[f] *Donahue and Prinn* [1990], 15°S marine boundary layer.
[g] Sum of calculated interferences due to RCH_2O_2, R_2CHO_2, and R_3CO_2.

before sampling. The latter result is obtained from the pressure- and temperature-dependent rate coefficients for HNO_4 production and thermal dissociation recommended by *Atkinson et al.* [1989]; we neglect other removal reactions of HNO_4. After expansion through the sampling nozzle and transit through the low-pressure flow tube for t_r = 25 ms, which is an upper limit to the transit time for air reaching the detection zone, part of the HNO_4 dissociates, part of the resulting HO_2 reacts with NO to form HO, and part of the HO reacts with NO or isobutane. Implicit integration of the differential equations for HNO_4, HO_2, and HO gives an estimate of the consequent interference. The yield of new HO_2 from the dissociation of HNO_4 during transit is 1.4% of the value of ambient [HO_2] immediately after expansion through the sampling nozzle. At the standard NO and isobutane reagent concentrations, the net modulated interference from this added HO_2 is 9×10^{-3} times the net signal from ambient HO_2. Thus an upper limit to the HNO_4 interference, under the above extreme steady state ambient conditions, is 1% of the signal from ambient [HO_2], and is thus negligible. For comparison, if we were to perform the HO_2 measurement in a 1 atm flow tube with the same 25 ms residence time, using NO and isobutane reagent concentrations reduced in inverse proportion to the pressure, the HNO_4 interference would grow to 40% of the signal from ambient HO_2.

Moreover, even under perturbed ambient conditions, the reaction $HO_2 + NO_2 + M \rightarrow HNO_4 + M$ is the only known source of atmospheric HNO_4. If HO_2 is removed by a perturbation (such as either mixing of NO from local sources or attenuation of daylight), then a corresponding decline in HNO_4 (by thermal dissociation) ensues with a characteristic time of 5 min at 273 K, or shorter times at higher temperatures. Thus the absolute value of the HNO_4 interference cannot be greater than that which existed before the perturbation, and cannot approach the value of perturbed [HO_2] unless the latter drops by a factor of at least 100 in a time much shorter than 5 min. Except for the latter restriction, we conclude that HNO_4 interference in the detection of HO_2 by FAGE is not significant in either polluted or remote tropospheric air at ground level, for either steady state or perturbed external conditions.

3. Laser photolysis of ambient O_3 (in the presence of H-containing species), H_2O_2, organic hydroperoxides, HNO_3, or HONO, can produce HO, leading to an HO-resonant background. As demonstrated elsewhere [*Hard et al.*, 1992], HO-resonant backgrounds arising from laser photolysis are modulated via the isobutane reagent's effects on fluorescence efficiency, resulting in a very small positive interference contribution. In the case of O_3, a larger negative interference results from the reaction of isobutane with $O(^1D)$. The absolute value of this dominant negative offset under the present conditions is less than −1% of peak daytime HO_2. Laser-photolytic interferences of this type other than O_3 have been treated by *Smith and Crosley* [1990] and are completely negligible for HO_2 measurements.

4. Other laser photolysis paths, such as $CH_2O+h\nu$, produce H atoms, which react with O_2 to produce HO_2 at a rate too slow to be significant (τ=555 ms at 4 torr). Moreover, during its brief residence time in the FAGE2 laser excitation zone, conversion of the HO_2 product to HO via reaction (R1) proceeds to only 1.4% of the conversion of ambient HO_2. The latter consideration likewise applies to any photolysis path that produces HO_2 directly.

5. Laser photolysis of ozone or NO_2 at 282 nm produces O atoms, which react with alkenes to give partial yields of the vinoxy radical CH_2CHO, which reacts with O_2 to yield HO [*Atkinson and Lloyd*, 1984]:

(R10) $CH_2CHO + O_2 \rightarrow HCHO + CO + HO$

Reaction (R10), driven by sunlight photolysis, may contribute slightly to ambient HO; however, the time constant for (R10) at 4 torr is 380 μs, too slow to contribute significant HO during the brief period of laser excitation, relative to the net HO signal from HO_2.

6. Laser photolysis of the HONO produced in reaction (R2) recreates HO. In the absence of isobutane, this HO production increases $(E_{c0})_{max}$ by a multiplicative factor greater than 1 but much less than 2. Since (R3) competes with (R2) for the HO product of (R1), modulation with isobutane leads to a similar, but smaller, multiplicative increase in E_{chem}. This minor multiplicative enhancement of the HO_2 response is independent of ambient conditions, and is not an interference since it is implicitly accounted for in the calibration procedure. No zero offset arises from this mechanism.

7. Production of HONO or HNO_3 by wall reactions between the reagent NO and adsorbed or gas-phase constituents leads to an observed photolytic source of false HO that is more significant than the other photolytic sources (3 through 6 above). We observed this effect by injecting high reagent NO concentrations into the HO_2 probe, resulting in a strong spectroscopic signal. This signal proved to be HO-resonant, proportional to reagent NO flow, and roughly proportional to the square of the laser power. The squared dependence indicates that this interference source is photolytic, i.e., one laser photon photodissociates a precursor to produce HO which is then detected by a second photon in the same laser pulse. This signal persisted even when the NO reagent was filtered successively by NaOH pellets, ascarite, and $FeSO_4$, and when the sample air was supplied by a pure air generator. One conceivable reaction sequence initiated by the reagent NO is

(R11) $2NO + O_2 \rightarrow 2NO_2$

(R12) $2NO_2 + H_2O \rightarrow HNO_3 + HONO$

where (R11), negligible in the gas phase at 4 torr, may occur on the wall. Reaction (R12) has been documented to occur in smog chambers [*Carter et al.*, 1982]. This photolytic HO source is the reason why we use $[NO]_{std} < [NO((E_{c0})_{max})]$, and why we modulate with isobutane with constant NO injection. Since NO flows in both sample probes, this HO source is present as a background which is largely subtracted out when the channel with the isobutane is subtracted from the signal channel. Since it raises the total background, it may degrade the instrument's sensitivity. The only net interference comes from quenching of this photolytic HO signal by the isobutane modulating reagent in the background channel. This reduces the background slightly in the channel with the isobutane, producing a net false positive signal that is known from other measurements to be two decades below the gross photolytic background, and is below the detection limit under standard instrumental conditions. However, if either chemical modulation with NO or spectral modulation were used instead of isobutane modulation, the interference would be approximately $+3\times10^6$ cm^{-3}, based on measurements with FAGE2. This is lower than the ambient

daytime peak HO_2 concentration of 1.6×10^7 cm^{-3} we observed on 2 days in 1983 with FAGE1 [*Hard et al.*, 1984] using NO modulation and is comparable with the uncertainty in $[HO_2]$ in the latter measurements.

Reduction of Interferences

It is desirable to further reduce contributions to the HO_2 signal from RO_2 species (estimated at 20% here), as well as any other significant interferences, in future measurements. Regarding the RO_2 interference source, Figure 6 shows that by lowering E_{chem} for HO_2, RO_2 interference could be further reduced by a reduction in the reagent [NO]. This approach would require an increase in signal averaging times but would be acceptable in many applications. If maximum HO_2 response (and therefore optimum time resolution) is required, then we can exploit the [M]-dependence of the RO_2 interference by varying the cell pressure, adjusting [NO] and [isobutane] as necessary to retain the desired E_{chem}. A reduction in the FAGE internal pressure from 4 to 2 torr, via a twofold reduction in nozzle area (keeping the same transit time t_r and adjusting reagent concentrations to maintain the same HO_2 conversion and modulation), yields a 62% decrease in the upper-limit daytime RO_2 interference from 20% to less than 8%.

Interference sources 2 and 6 above are negligible. Sources 3, 4, 5, and 7, which are proportional to the first power of the laser flux, are greatly reduced by the use of the FAGE3 instrument [*Chan et al.*, 1990], in which a copper-laser-pumped dye laser delivers lower pulsed flux and higher pulse repetition rate than the YAG/dye laser used above.

COMPARISON WITH MODEL PREDICTIONS AND OTHER MEASUREMENTS

Logan et al. [1981] predicted HO_2 concentrations of 3.3×10^8 cm^{-3} (45°N latitude, 0 km altitude, equinox) at the midday maximum and 1 to 10 $\times10^6$ cm^{-3} at night. For the marine boundary layer at 40°N *Madronich and Calvert* [1990] predicted HO_2 concentrations of 3.2×10^8 cm^{-3} at noon. For the tropical remote MBL at 15°S, *Donahue and Prinn* [1990] predicted $[HO_2]$ of 4×10^8 cm^{-3} at the daytime maximum and 5×10^7 cm^{-3} at night.

Mihelcic et al. [1990] observed an HO_2 level of 38 pptv (8.3×10^8 cm^{-3}) at midday at a mountain site (Schauinsland, 1150 m altitude, 48°N) in the Black Forest, via numerical deconvolution of peroxy-radical ESR spectra in cryocondensed samples. Approximately 1 hour earlier the same day, Mihelcic et al. found 13 pptv HO_2, 86 pptv alkyl-RO_2, and 16 pptv CH_3CO_3.

Cantrell and Stedman [1982] employed a peroxy-radical chemical amplifier (PERCA) to measure a weighted sum of HO_2 and RO_2. The amplifier was based upon reaction (R1), driven by an added excess of NO reagent, and

$$\text{(R13)} \qquad HO + CO + O_2 \rightarrow HO_2 + CO_2$$

for which excess CO was also added. This cyclic reaction chain regenerates HO_2 and accumulates NO_2. The NO and CO concentrations were adjusted to achieve sufficient chain length to allow detection of the NO_2 product. RO_2 contributed to NO_2 via generation of HO_2 via (R5*a*) and (R6), followed by the above chain. Experiments at the rooftop of the National Center for Atmospheric Research in Boulder, Colorado, yielded daytime peroxy radical signals ranging from below 1×10^9 cm^{-3} to 2×10^{10} cm^{-3}.

Parrish et al. [1986] measured the sum of oxidants O_X other than ozone which contribute to the oxidation of atmospheric NO to NO_2. In the absence of such oxidants, the photochemical steady state expression is

$$j_{NO2}[NO_2]/(k_{NO+O3}[NO][O_3]) = 1$$

Parrish et al. measured O_X as the discrepancy

$$[O_X] = j_{NO2}[NO_2]/(k_{NO+O3}[NO]) - [O_3]$$

which can be caused either by significant contributions from (R1) and (R5*a*) + (R6) or other chemical processes, or by non-steady state kinetics due to local sources of NO_x (which were presumed absent). At Niwot Ridge, Colorado, they observed average summer midday O_X of 60 ppb in units of equivalent ozone concentration, which would be equal to 3.5×10^9 cm^{-3} (142 pptv) if the excess oxidant were assumed to consist entirely of HO_2.

Taken as HO_2, the oxidant concentrations detected indirectly in surface air by Cantrell and Stedman and by Parrish et al. were more than one decade higher than the directly detected HO_2 concentrations reported by *Mihelcic et al.* [1990], *Hard et al.* [1984], and in the present work. This difference is worthy of further study.

SUMMARY: MEASUREMENT ACCURACY, PRECISION, AND UNCERTAINTY

Based upon multiple calibration determinations, we assign a random calibration uncertainty of ±30% (see above). Improvement in this uncertainty could be obtained by finding calibration conditions which would extend the linearity of the curves in Figure 5 by reducing the first-order HO_2 removal process. An additional systematic error of 30% is associated with the uncertainty in the rate constants $k_{4a}+k_{4b}$. Uncertainties in the chemical conversion and modulation efficiencies are attributable to uncertainties in the governing rate constants (equations (1)-(5)), as well as to a possible contribution to heterogeneous processes in HO_2 reduction to HO or in subsequent HO loss. Since these conversion efficiencies are calculated only for the purpose of instrument design, and since their effects are incorporated into the calibration procedure, they do not introduce any additional uncertainty per se. Another source of error in the HO_2 measurement arises from the photon counting statistics of the acquired signal. The statistics for FAGE2 HO measurements have been discussed in detail by *Hard et al.* [1992]. The only difference in their application to HO_2 lies in the larger relative HO_2 concentration, which allows shorter averaging times than with HO. For the present paper an averaging time of 0.1 hour has been chosen, and the resultant signal uncertainty is <10%. Shorter averaging times would clearly give acceptable signal-to-noise ratio as well. The resultant of the random calibration uncertainty, the rate coefficient uncertainty, and the ambient HO_2 signal uncertainty, $(0.30^2+0.30^2+0.10^2)^{1/2}$, is an estimated overall uncertainty of 44%. An additional source of systematic uncertainty lies in the potential contribution of RO_2 species to the HO_2 signal. These interferences have been estimated here from kinetic theory, with appropriate RO_2 concentrations from atmospheric models. The estimates (Table 3) indicate the HO_2 concentrations we measured in daytime at 45° N may be 20% high due to RO_2 contributions, and larger RO_2 interferences (relative to $[HO_2]$) are expected at night. Adjustment of measurement conditions to optimize for HO_2 selectivity was discussed

above, and future measurements will minimize the relative response from RO_2.

CONCLUSION

We have observed the diurnal cycle of atmospheric HO_2 at coastal and urban sites near the Earth's surface. We have achieved self-calibration of the instrument by the self-decay of HO_2. We have considered several possible interferences. The observed small nighttime signals at both sites may contain, besides ambient HO_2, significant contributions from interferences by RO_2. The lowest nighttime HO_2 signals observed, before midnight August 26 and after 0600 August 27, 1987 (Figure 4), are indicative of the low level of positive photolytic signal associated with the NO reagent (interference 7 above). With a change to lower laser pulse energy and higher repetition rate, the only known remaining interference is due to RO_2, which model calculations suggest may contribute 20% of the observed daytime HO_2 signal and more than half of the signal at night. The RO_2 interference can be reduced to less than 3% of concurrent daytime maximum HO_2 (and 10% of nighttime HO_2) by changes in the operating parameters of FAGE.

Acknowledgments. This work was supported by National Science Foundation grant ATM-8615163, National Aeronautics and Space Administration grant NAG-1-697, and Environmental Protection Agency grant R81-3012. This is Environmental Sciences and Resources Publication 271. We are grateful to James Greenberg and the National Center for Atmospheric Research for providing the HC sampling apparatus and for performing the hydrocarbon analyses.

REFERENCES

Anderson, J. G., H. J. Grassl, R. E. Shetter, and J. J. Margitan, HO_2 in the stratosphere: Three in situ observations, *Geophys. Res. Lett., 8*, 289-292, 1981.

Atkinson, R., and A. C. Lloyd, Evaluation of kinetic and mechanistic data for modeling of photochemical smog, *J. Phys. Chem. Ref. Data, 13*, 315-444, 1984.

Atkinson, R., D. L. Baulch, R. A. Cox, R. F. Hampson, Jr., J. A. Kerr, and J. Troe, Evaluated kinetic and photochemical data for atmospheric chemistry: Supplement III, *J. Phys. Chem. Ref. Data., 18*, 1081-1097, 1989.

Cantrell, C. A., and D. H. Stedman, A possible technique for the measurement of atmospheric peroxy radicals, *Geophys. Res. Lett., 9*, 846-849, 1982.

Carter, W. P. L., R. Atkinson, A. M. Winer, and J. N. Pitts, Jr., Experimental investigation of chamber dependent radical sources, *Int. J. Chem. Kinet., 14*, 1071-1103, 1982.

Chameides, W. L., and D. D. Davis, The free-radical chemistry of cloud droplets and its impact upon the composition of rain, *J. Geophys. Res., 87*, 4863-4877, 1982.

Chan, C. Y., T. M. Hard, A. A. Mehrabzadeh, L. A. George, and R. J. O'Brien, Third-generation FAGE instrument for tropospheric hydroxyl measurements, *J. Geophys. Res., 95*, 18569-18576, 1990.

Darnall, K. R., R. Atkinson, and J. N. Pitts, Rate constants for the reaction of the OH radical with selected alkanes at 300 K, *J. Chem. Phys., 82*, 1581-1584, 1978.

Donahue, N. M., and R. G. Prinn, Nonmethane hydrocarbon chemistry in the remote marine boundary layer, *J. Geophys. Res., 95*, 18387-18411, 1990.

Fitzgerald, G., T. J. Lee, H. F. Schaefer III, and R. J. Bartlett, The open chain or chemically bonded structure of H_2O_4: The hydroperoxyl radical dimer, *J. Chem. Phys., 83*, 6275-6281, 1985.

Greenberg, J. P., and P. R. Zimmerman, Nonmethane hydrocarbons in remote tropical, continental and marine atmospheres, *J. Geophys. Res., 89*, 4767-4778, 1984.

Greiner, N. R., Hydroxyl radical kinetics by kinetic spectroscopy, VI, Reactions with alkanes in the range 300-500 K, *J. Chem. Phys., 53*, 1070-1076, 1970.

Hard, T. M., R. J. O'Brien, C. Y. Chan, and A. A. Mehrabzadeh, Tropospheric free radical determination by FAGE, *Environ. Sci. Technol., 18*, 768-777, 1984.

Hard, T. M., C. Y. Chan, A. A. Mehrabzadeh, W. H. Pan, and R. J. O'Brien, Diurnal cycle of tropospheric OH, *Nature, 322*, 617-620, 1986.

Hard, T. M., A. A. Mehrabzadeh, C. Y. Chan, and R. J. O'Brien, FAGE measurements of tropospheric HO: Ambient data, with model and measurements of interferences, *J. Geophys. Res.*, in press, 1992.

Jacob, D. J., Chemistry of OH in remote clouds and its role in the production of formic acid and peroxymonosulfate, *J. Geophys. Res., 91*, 9807-9826, 1986.

Lelieveld, J., and P. J. Crutzen, Influences of cloud photochemical processes on tropospheric ozone, *Nature, 343*, 227-233, 1990.

Logan, J. A., M. J. Prather, S. C. Wofsy, and M. B. McElroy, Tropospheric chemistry: A global perspective, *J. Geophys. Res., 86*, 7210-7254, 1981.

Madronich, S., and J. G. Calvert, Permutation reactions of organic peroxy radicals in the troposphere, *J. Geophys. Res., 95*, 5697-5715, 1990.

Mihelcic, D., D. H. Ehhalt, J. Klomfass, G. F. Kulessa, U. Schmidt, and M. Trainer, Measurements of free radicals in the atmosphere by matrix isolation and electron paramagnetic resonance, *Ber. Bunsen Ges. Phys. Chem., 82*, 16-19, 1978.

Mihelcic, D., P. Müsgen, and D. H. Ehhalt, An improved method of measuring tropospheric NO_2 and RO_2 by matrix isolation and electron spin resonance, *J. Atmos. Chem., 3*, 341-361, 1985.

Mihelcic, D., A. Volz-Thomas, H. W. Pätz, D. Kley, and M. Mihelcic, Numerical analysis of ESR spectra from atmospheric samples, *J. Atmos. Chem., 11*, 271-297, 1990.

Mozurkewich, M., P. H. McMurry, A. Gupta, and J. G. Calvert, Mass accommodation coefficients for HO_2 radicals on aqueous particles, *J. Geophys. Res., 92*, 4163-4170, 1987.

Parrish, D. D., M. Trainer, E. J. Williams, D. W. Fahey, G. Huebler, C. S. Eubank, S. C. Liu, P. C. Murphy, D. L. Albritton, F. C. Fehsenfeld, Measurements of the nitrogen oxide (NO_x)-ozone photostationary state at Niwot Ridge, Colorado, *J. Geophys. Res., 91*, 5361-5370, 1986.

Sander, S. P., M. Peterson, R. T. Watson, and R. Patrick, Kinetics studies of the HO_2 and DO_2 reactions at 298 K, *J. Phys. Chem., 86*, 1236-1240, 1982.

Schwartz, S. E., Gas- and aqueous-phase chemistry of HO_2 in liquid water clouds, *J. Geophys. Res., 89*, 11589-11598, 1984.

Smith, G. P., and D. R. Crosley, A photochemical model of interference effects in laser detection of tropospheric OH, *J. Geophys. Res., 95*, 16427-16442, 1990.

Stimpfle, R. M., P. O. Wennberg, L. B. Lapson, and J. G. Anderson, Simultaneous in situ measurements of OH and HO_2 in the stratosphere, *Geophys. Res. Lett., 17*, 1905-1908, 1990.

Traub, W. A., D. G. Johnson, and K. V. Chance, Stratospheric hydroperoxyl measurements, *Science, 247*, 446-449, 1990.

C. Y. Chan, T. M. Hard, A. A. Mehrabzadeh, and R. J. O'Brien, Chemistry Department, Portland State University, P. O. Box 751, Portland, Oregon 97207-0751.

(Received July 16, 1991;
revised January 30,1991;
accepted January 30, 1991.)